

Valley selecting current partition at zero-line mode of quantum anomalous Hall topologies

Ma Luo*

*The State Key Laboratory of Optoelectronic Materials and Technologies
School of Physics*

Sun Yat-Sen University, Guangzhou, 510275, P.R. China

Zero-line mode of monolayer graphene in quantum anomalous Hall phase has been proposed. In the presence of staggered sublattice potential, the band gaps of the two valleys become different, and the phase diagram of the topological Chern number has an additional topological trivial regime. The domain wall between topological trivial and non-trivial regions support zero-line mode in only one valley. The nano-devices consisted of Y-shape junctions of three zero-line modes exhibit the functions of valley splitting, merging or filtering for the incident currents.

PACS numbers: 81.05.ue, 78.67.Wj, 73.22.Pr, 72.80.Vp

I. INTRODUCTION

Investigation of the quantum anomalous Hall(QAH) effect in two dimensional materials has been attracting vast interest[1–6, 8–12, 22]. Single layer graphenes in the presence of the Rashba spin-orbital coupling (SOC) and the exchange field exhibit QAH effect. The quantized charge Hall conductance is determined by the Chern number, which label the global property of the band structure. Because of the topological non-trivial property of the band structure, at the edge of the graphene nano-ribbon, the robust gapless edge states appear. Another type of edge states appear at the interface between two topological non-trivial insulator with different topological invariants, which is call the zero-line mode(ZLM)[13–20]. The ZLMs is localized near to the interface and propagating along the interface. The ZLM have been theoretically described in single layer graphene with stagger sublattice potential and gated bilayer graphene. Current partition at the junction of four ZLMs splits the incident current into two currents[21–25]. The prediction of the optical excitation of localized spin and valley currents promote the ZLMs as promising candidate for integrated optical spintronic and valleytronic devices[26]. The ZLMs have been experimentally implemented recently. Comparing to these two types of ZLMs, the ZLM at the interface between two single layer graphene in QAH phase with opposite Chern number has different properties[25]. The dispersions at K and K' valleys are the same, due to the breaking of the time reversal symmetric by the exchange field. Current partition at this type of ZLM exhibit similar rules.

On the other hand, the staggered sublattice potential in the graphene open a band gap. This potential could be realized by h-BN [27, 28] or SiC [29] substrates. Combination of the staggered sublattice potential with the gate bilayer graphene exhibit diversified

phase diagram[30, 31]. Novel type of ZLMs are predicted in this system[32]. In this paper, we combine the staggered sublattice potential with the single layer graphene with Rashba SOC and exchange field. In the absence of the staggered sublattice potential, the graphene is in the QAH phase. The presence of the staggered sublattice potential modified the phase diagram, as shown in the following discussion. The ZLMs at the interface between topological trivial and non-trivial phase is investigated. Because of the diversification of the phase diagram, Y-shape junction between three ZLMs is allowed. The Y-shape junction exhibit valley selecting current partition, which can be used to construct valley splitting, merging or filtering devices.

The article is organized as following: In section II, the tight binding model for the graphene with Rashba SOC, exchange field and staggered sublattice potential is given. The phase diagram and band structure of the bulk graphene is discussed in this section. In section III, the band structure of the ZLMs in the middle of the zigzag-edge nano-ribbon is calculated. In section IV, the Y-shape junctions are proposed. The two devices with valley splitting(merging) and filtering effects are simulated by applying the non-equilibrium Green's function method. In section V, the conclusion is given.

II. QUANTUM ANOMALOUS HALL TOPOLOGIES WITH STAGGERED SUBLATTICE POTENTIAL

The tight binding Hamiltonian of the graphene with exchange field and staggered sublattice potential is given as

$$\begin{aligned}
 H = & -t \sum_{\langle i,j \rangle, \alpha} c_{i\alpha}^+ c_{j\alpha} \\
 & + igR \sum_{\langle i,j \rangle, \alpha, \beta} c_{i\alpha}^+ [(\mathbf{S} \times \mathbf{d}_{ij}) \cdot \hat{\mathbf{z}}]_{\alpha\beta} c_{j\beta} \\
 & + \lambda \sum_{i, \alpha} c_{i\alpha}^+ \sigma_z c_{i\alpha} + \Delta \sum_{i, \alpha} \delta_i c_{i\alpha}^+ c_{i\alpha} \quad (1)
 \end{aligned}$$

*Corresponding author: luom28@mail.sysu.edu.cn

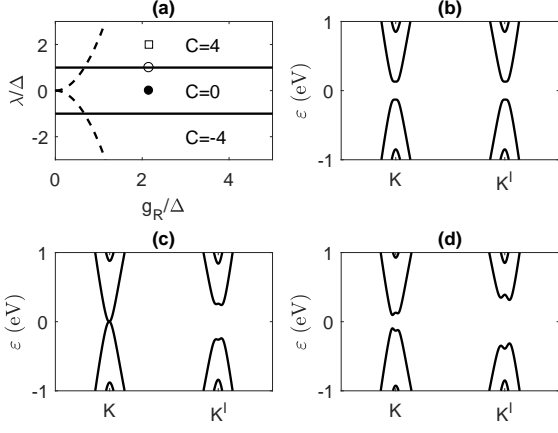


FIG. 1: (a) The phase diagram of the graphene in the λ/Δ - g_R/Δ space. The solid line separate different phase, and the dash lines separate regimes with different type of band gap at K and K' points. (b) (c) and (d) are the bulk band structure of the graphene in the phases labeled by the filled circle, empty circle and empty square in (a), respectively.

where i and j label the lattice sites, $\alpha = \pm 1$ and $\beta = \pm 1$ label the spin projections, the summations with index $\langle i, j \rangle$ run through the nearest neighboring sites, $t = 2.8$ eV is the nearest neighbor hopping energy, g_R is the Rashba SOC strength, λ is the exchange field strength, Δ is the staggered sublattice potential magnitude, $\delta_i = +1(-1)$ for $i \in A(B)$, \mathbf{S} is vector of Pauli matrix, \mathbf{d}_{ij} is the unit vector from lattice i to j , $\sigma_z = \pm 1$ is the spin z projection.

Applying the Bloch periodic boundary condition, the bulk band structure is obtained. The topological phase is determined by the Chern number, which is the integral of the Berry curvature through the whole Brillouin zone. The phase diagram is plotted in Fig. 1(a). The phase transition boundaries are featured by gap closing, which occur at K or K' point. In the simultaneous presence of the staggered sublattice potential and exchange field, the band structures in K and K' valley are different. Specifically, the eigenvalues at $K(K')$ point are $\pm[\Delta + (-)\lambda]$ and $\pm\sqrt{g_R^2 + (\Delta - (+)\lambda)^2}$. In the regime with $\lambda > (<) + (-)9g_R^2/(4\Delta)$ (to the left of the dash line in Fig. 1(a)), the band gap at $K(K')$ point is $2\sqrt{g_R^2 + (\Delta - (+)\lambda)^2}$; in the other regime, the band gap at $K(K')$ point is $2[\Delta + (-)\lambda]$. Thus, the band gap at $K(K')$ point is closed when $\lambda = -(+)\Delta$ for arbitrary g_R , or when $g_R = 0$ and $\lambda = +(-)\Delta$. The global band gap is close at two solid lines in Fig. 1(a), which separate the topological trivial and non-trivial phases. The band structures of three typical systems with parameter being labeled in Fig. 1(a) are plotted in 1(b), (c) and (d), respectively. In the trivial phase with $\lambda = 0$, the band structures of K and K' valleys are the same, as shown in Fig. 1(b). The band gap is 2Δ . Increasing

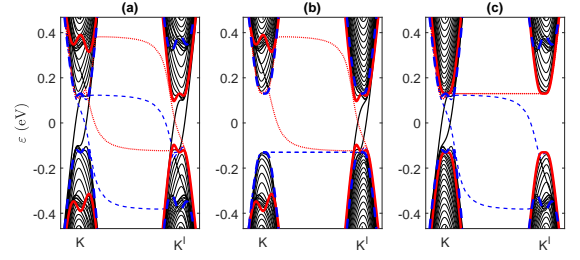


FIG. 2: Band structure of zigzag-edge nano-ribbon with $g_R = 0.2t$ and $\Delta = 130meV$. The exchange field at the left and right half of the nano-ribbon is $\lambda = +2\Delta$ and $\lambda = -2\Delta$ in (a), $\lambda = +2\Delta$ and $\lambda = 0$ in (b), $\lambda = 0$ and $\lambda = -2\Delta$ in (c). The total width of the nano-ribbon is 51.12 nm. The ZLM localized in the middle of the nano-ribbon is plotted as black(solid) lines, the edge mode localized at the left zigzag edge is plotted as red(dotted) lines and the edge mode localized at the right zigzag edge is plotted as blue(dashed) lines. The thick red(solid) and blue(dashed) lines are the bulk band edge of the left and right regions, respectively. The thin black(solid) lines are bulk states.

ing λ drives the band gap in $K(K')$ point smaller(larger). With $\lambda = \Delta$, the gap at K point is closed, as shown in Fig. 1(c). Further increasing λ reopen the gap at K point. With $\lambda = 2\Delta$, the band gap at K point reaches 2Δ again, as shown in Fig. 1(d). Note that the global band gap is slightly smaller than 2Δ , because the band minimal locate beyond the K point. Flipping the sign of the exchange field exchange the band structures at K and K' points. As a result, the electron transportation and optical excitation in these graphenes exhibit valley selecting property that is controlled by the exchange field.

The ZLMs are form at the interface between two regions with different Chern numbers. In order to exhibit the ZLMs numerically, we calculate the band structures of zigzag-edge nano-ribbons. The domain wall locate along the ribbon extending direction in the middle of the ribbon. When the exchange field at the left and right half of the nano-ribbon is $\lambda = +2\Delta$ and $\lambda = -2\Delta$, the band structure is shown in Fig. 2(a). The ZLMs at the two valleys have the same dispersion. In addition to the ZLMs, the edge states localized at the left and right edges are also gapless, and have dispersion opposite being opposite to the ZLMs. Erasing the exchange field at the right half eliminates the ZLMs in K valley, as shown in Fig. 2(b). Meanwhile the edge states localized at the right edges become two-fold degenerated flat band. Erasing the exchange field at the left half has similar effect, as shown in Fig. 2(c). The numerical result of the band structures confirm that the number of gapless edge states at the interface between two regions is determined by the difference between the Chern numbers.

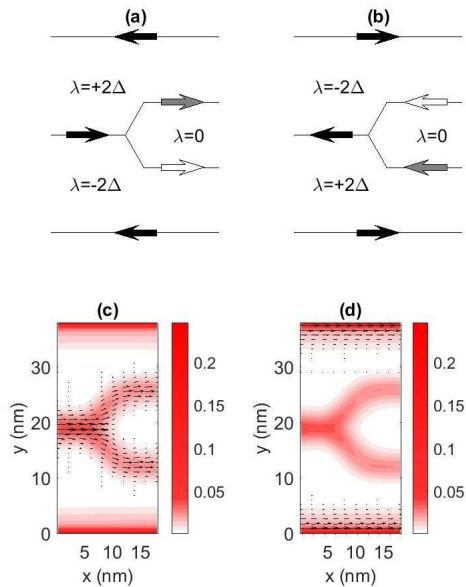


FIG. 3: (a) and (b) are spatial blueprint of the Y-shape junction in a nano-ribbon. The exchange fields of each region in (a) and (b) are opposite to each other. The black arrow indicate edge current in both valley, the white(grey) arrow indicate valley polarized edge current in K(K') valley. (c) and (d) are the numerical result of the transportation calculation of the systems in (a) and (b) under forward bias, respectively. The shaded plots indicate the local density of state, and the vector fields indicate the local current distribution.

III. VALLEY SPLITTING CURRENT PARTITION

Because changing the exchange field drives the graphene into three topological phase with different Chern number, the interfaces between any two phases support the ZLMs. The Y-shape junction of three ZLMs has the function of current partition. Denote the three type of ZLMs in Fig. 2(a), (b) and (c) as ZLM-a, ZLM-b and ZLM-c.

The nano-structure with valley splitting effect is presented in Fig. 3(a). Because the ZLM-b and ZLM-c only support current in K and K' valley, respectively, under forward bias, the incident charge current from the ZLM-a are split into two currents. Because all ZLMs have positive dispersion, the backward bias does not excite current in the ZLMs, but excite currents along the edge. Flipping the sign of the exchange field at all regions gives the nano-structure with valley merging effect, as shown in Fig. 3(b). In this case, the forward bias excite currents along the edge; the backward bias excite valley polarized current at ZLM-b and ZLM-c, which merge at the Y-shape junction. The proposal are confirmed by numerical calculation of quantum transportation based on the non-equilibrium Green's function theory[33–37]. The front and back leads are the nano-ribbons with one and two domain walls, respectively; the Y-shape junction is

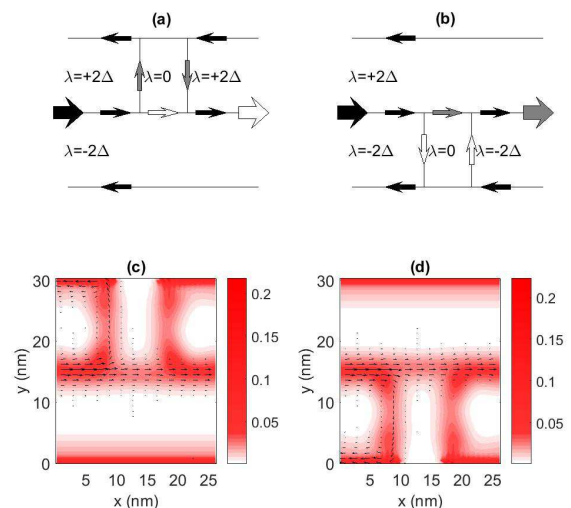


FIG. 4: The same type of plotting as in Fig. 3 for the valley filtering devices. In (a) and (b), the wider black arrow indicate the incident charge current; the wider white(grey) arrow indicate the exiting valley polarized current at K(K') valley at the ZLMs that support current in both valley.

the scattering region. The local density of state is given by the imaginary part of the retarded Green's function as $-\frac{1}{2\pi}Im[G^r(\mathbf{r})]$. The local current is given as

$$\mathbf{j}(\mathbf{r}_i \rightarrow \mathbf{r}_j) = -\frac{2e\hat{\mathbf{d}}_{ij}}{h} \int dE [t_{ij}G^<(\mathbf{r}_j, \mathbf{r}_i) - t_{ji}G^<(\mathbf{r}_i, \mathbf{r}_j)] \quad (2)$$

where \mathbf{r}_i is the position of the i-th lattice site, $\hat{\mathbf{d}}_{ij}$ is the unit vector from the i-th to j-th lattice site, e is the electron charge, h is the Planck constant, t_{ij} is the hopping parameter between the i-th and j-th lattice site, and $G^<(\mathbf{r}_i, \mathbf{r}_j)$ is the lesser Green's function. The numerical results are plotted in Fig. 3(c) and (d) for the Y-shape junction in Fig. 3(a) and (b), respectively. Both figures present the results with forward bias. Under backward bias, the current distributions of the system in Fig. 3(a) and (b) are given by the result in Fig. 3(d) and (c) with reversing current direction, respectively. The results that the system in Fig. 3(a) has valley splitting effect under forward bias, and exhibit regular edge transportation under backward bias. In contrary, the system in Fig. 3(b) has valley merging effect under backward bias, and exhibit regular edge transportation under forward bias.

Although the ZLM-a support current in both valley, excitation of valley polarized current in ZLM-a could be useful for valleytronic devices. The valley filtering devices consisting of two Y-shape junction is presented in Fig. 4(a) and (b). The background of the nano-structure is the nano-ribbon with ZLM-a. In the scattering region, a square with $\lambda = 0$ presents at the $\lambda = +2\Delta$ and $\lambda = -2\Delta$ half in Fig. 4(a) and (b), respectively. Because the edge states at the open boundary of the $\lambda = 0$ piece is gapped flat band, this section of the zigzag edge does not sup-

port current. The K(K') valley current transmit through the ZLM-c(ZLM-b), and excite the valley polarized current at the exiting lead; the K'(K) valley current turn around into the edge states and return to the entering lead. The devices effectively transmit the K(K') valley current and back-scatter the K'(K) valley current, which form the K(K') valley filter. The proposal is confirmed by the quantum transportation calculation as well, which is plotted in Fig. 4(c) and (d).

IV. CONCLUSION

In summary, the ZLMs based on single layer graphene with QAH phase and the presence of the staggered sublattice potential is studied. Two additional types of ZLMs are identified, which support current in K or K' valley only. The Y-shape current partition at the junction of three different type of ZLMs are proposed. The devices with valley splitting, merging and filtering effects are designed. The valley splitting device generates entan-

gle quantum states at two ZLMs, which should be further investigated as possible candidate of building block of quantum computational devices. The valley filtering device makes integrated valleytronic feasible. All devices can be controlled by the distribution of the exchange field, which favor the development of the programable integrated devices.

Acknowledgments

The project is supported by the National Natural Science Foundation of China (Grant: 11704419), the National Basic Research Program of China (Grant: 2013CB933601), and the National Key Research and Development Project of China (Grant: 2016YFA0202001).

References

-
- [1] Rui Yu, Wei Zhang, Hai-Jun Zhang, Shou-Cheng Zhang, Xi Dai, Zhong Fang, *Science*, 329, 61(2010).
 - [2] Zhenhua Qiao, Shengyuan A. Yang, Wanxiang Feng, Wang-Kong Tse, Jun Ding, Yugui Yao, Jian Wang, and Qian Niu, *Phys. Rev. B* 82, 161414(R)(2010).
 - [3] Wang-Kong Tse, Zhenhua Qiao, Yugui Yao, A. H. MacDonald, and Qian Niu, *Phys. Rev. B* 83, 155447(2011).
 - [4] Hongbin Zhang, Cesar Lazo, Stefan Blugel, Stefan Heinze, and Yuriy Mokrousov, *Phys. Rev. Lett.* 108, 056802(2012).
 - [5] Z. F. Wang, Zheng Liu, and Feng Liu, *Phys. Rev. Lett.* 110, 196801(2013).
 - [6] Shu-Chun Wu, Guangcun Shan, and Binghai Yan, *Phys. Rev. Lett.* 113, 256401(2014).
 - [7] Zhenhua Qiao, Wei Ren, Hua Chen, L. Bellaiche, Zhenyu Zhang, A. H. MacDonald, and Qian Niu, *Phys. Rev. Lett.* 112, 116404(2014).
 - [8] Gang Xu, Biao Lian, and Shou-Cheng Zhang, *Phys. Rev. Lett.* 115, 186802(2015).
 - [9] J. L. Lado and J. Fernandez-Rossier, *Phys. Rev. B* 92, 115433(2015).
 - [10] Shifei Qi, Zhenhua Qiao, Xinzhou Deng, Ekin D. Cubuk, Hua Chen, Wenguang Zhu, Efthimios Kaxiras, S. B. Zhang, Xiaohong Xu, and Zhenyu Zhang, *Phys. Rev. Lett.* 117, 056804(2016).
 - [11] Jian Zhou, Qi-Feng Liang, Hongming Weng, Y. B. Chen, Shu-Hua Yao, Yan-Feng Chen, Jinming Dong, and Guang-Yu Guo, *Phys. Rev. Lett.* 116, 256601(2016).
 - [12] Liang Dong, Youngkuk Kim, Dequan Er, Andrew M. Rappe, and Vivek B. Shenoy, *Phys. Rev. Lett.* 116, 096601(2016).
 - [13] Ivar Martin, Ya. M. Blanter, and A. F. Morpurgo, *Phys. Rev. Lett.* 100, 036804(2008).
 - [14] Matthew Killi, Si Wu, and Arun Paramekanti, *Phys. Rev. Lett.* 107, 086801(2011).
 - [15] M. Zarenia, J. M. Pereira, Jr., G. A. Farias, and F. M. Peeters, *Phys. Rev. B* 84, 125451(2011).
 - [16] Jelena Klinovaja, Gerson J. Ferreira, and Daniel Loss, *Phys. Rev. B* 86, 235416(2012).
 - [17] Abolhassan Vaezi, Yufeng Liang, Darryl H. Ngai, Li Yang, and Eun-Ah Kim, *Phys. Rev. X* 3, 021018(2013).
 - [18] Fan Zhang, Allan H. MacDonald and Eugene J. Mele, *PNAS*, 110(26), 10546-10551(2013).
 - [19] Xintao Bi, Jeil Jung, and Zhenhua Qiao, *Phys. Rev. B* 92, 235421(2015).
 - [20] Changhee Lee, Gunn Kim, Jeil Jung, and Hongki Min, *Phys. Rev. B* 94, 125438(2016).
 - [21] Zhenhua Qiao, Jeil Jung, Qian Niu, and Allan H. MacDonald, *Nano Lett.*, 2011, 11 (8), 3453C3459(2011).
 - [22] Zhenhua Qiao, Jeil Jung, Chungwei Lin, Yafei Ren, Allan H. MacDonald, and Qian Niu, *Phys. Rev. Lett.* 112, 206601(2014).
 - [23] J. R. Anglin and A. Schulz, *Phys. Rev. B* 95, 045430(2017).
 - [24] Ke Wang, Yafei Ren, Xinzhou Deng, Shengyuan A. Yang, Jeil Jung, and Zhenhua Qiao, *Phys. Rev. B* 95, 245420(2017).
 - [25] Yafei Ren, Junjie Zeng, Ke Wang, Fuming Xu, and Zhenhua Qiao, *Phys. Rev. B* 96, 155445(2017).
 - [26] Ma Luo and Zhibing Li, *Phys. Rev. B* 96, 165424(2017).
 - [27] Gianluca Giovannetti, Petr A. Khomyakov, Geert Brocks, Paul J. Kelly, and Jeroen van den Brink, *Phys. Rev. B* 76, 073103(2007).
 - [28] C. R. Dean, A. F. Young, I. Meric, C. Lee, L. Wang, S. Sorgenfrei, K. Watanabe, T. Taniguchi, P. Kim, K. L. Shepard, and J. Hone, *Nat. Nanotechnol.* 5, 722 (2010).
 - [29] S. Y. Zhou, G.-H. Gweon, A. V. Fedorov, P. N. First, W. A. de Heer, D.-H. Lee, F. Guinea, A. H. Castro Neto, and A. Lanzara, *Nat. Mater.* 6, 770 (2007).
 - [30] Xuechao Zhai and Guojun Jin, *Phys. Rev. B* 93, 205427(2016).
 - [31] Ma Luo and Zhibing Li, arXiv:1804.07868 [cond-

- mat.mes-hall].
- [32] Ma Luo and Zhibing Li, arXiv:1804.07868 [cond-mat.mes-hall].
 - [33] M P Lopez Sancho, J M Lopez Sancho and J Rubio, Phys. F: Met. Phys., 14, 1205-1215(1984).
 - [34] Marco Buongiorno Nardelli, Phys. Rev. B, 60, 7828(1998).
 - [35] Fufang Xu, Baolei Li, Hui Pan, and Jia-Lin Zhu, Phys. Rev. B 75, 085431(2007).
 - [36] G. S. Diniz, A. Latg, and S. E. Ulloa, Phys. Rev. Lett. 108, 126601(2012).
 - [37] Caio H. Lewenkopf, Eduardo R. Mucciolo, J. Comput. Electron., 12, 203C231(2013).